

# Quantum Memory Hierarchies: Efficient Designs to Match Available Parallelism in Quantum Computing

Darshan D. Thaker<sup>†</sup> Tzvetan S. Metodi<sup>†</sup> Andrew W. Cross<sup>‡</sup> Isaac L. Chuang<sup>‡</sup> Frederic T. Chong<sup>\*</sup>

<sup>†</sup>University of California at Davis, One Shields Avenue, Davis, CA 95616, USA

<sup>‡</sup>Massachusetts Institute of Technology, 77 Massachusetts Avenue, Cambridge, MA 02139

<sup>\*</sup>University of California at Santa Barbara, Santa Barbara, CA 93106, USA

## Abstract

*The assumption of maximum parallelism support for the successful realization of scalable quantum computers has led to homogeneous, “sea-of-qubits” architectures. The resulting architectures overcome the primary challenges of reliability and scalability at the cost of physically unacceptable system area. We find that by exploiting the natural serialization at both the application and the physical microarchitecture level of a quantum computer, we can reduce the area requirement while improving performance. In particular we present a scalable quantum architecture design that employs specialization of the system into memory and computational regions, each individually optimized to match hardware support to the available parallelism. Through careful application and system analysis, we find that our new architecture can yield up to a factor of thirteen savings in area due to specialization. In addition, by providing a memory hierarchy design for quantum computers, we can increase time performance by a factor of eight. This result brings us closer to the realization of a quantum processor that can solve meaningful problems.*

## 1 Introduction

Conventional architectural design adheres to the concept of **balance**. For example, the register file depth is matched to the number of functional units, the memory bandwidth to the cache miss rate, or the interconnect bandwidth matched to the compute power of each element of a multiprocessor. We apply this concept to the design of a quantum computer and introduce the *Compressed Quantum Logic Array* (CQLA), an architecture that balances components and resources in terms of exploitable parallelism. The primary goal of our design is to address the problem of large area, approximately 1 m<sup>2</sup> on a side, of our previous design [1].

Specifically, we discover that the prevailing approach to designing a quantum computer, that of supporting maximal parallelism, is area inefficient. We also find that exploitable parallelism is inherently limited by both resource constraints and application structure. This lack of parallelism gives us the freedom to increase density by specializing components as blocks of memory and blocks of computation.

We introduce the idea of periodically reducing our investment in reliability and thereby increasing speed. By encoding the compute regions differently than memory we provide very fast compute regions, while allowing the memory to be slower and more reliable. To ensure that the faster compute region does not suffer from too many stalls, we employ a quantum memory hierarchy wherein the cache utilizes the same encoding mechanism as the compute region. When making this effort to improve speed, it is critical that overall system fidelity is maintained. We show how this can be accomplished.

Due to the quantum no-cloning theorem [2], it is necessary for all quantum data to physically move from source to destination. We cannot create a copy of the data and send the copy. Our architecture focuses on implementation with an array of trapped atomic ions, one of the most mature and scalable technologies that provides a wealth of experimental data. In ion-traps, the physical representation of data are ions that are in constant motion, on a two dimensional grid, throughout the computation. Since this physical movement is slow, yet unavoidable, it limits available parallelism at the microarchitecture level.

At the application level, we find that only a limited amount of parallelism can be extracted from key quantum algorithms. This means that we may only need a few compute blocks for all the qubits in memory. This is in contrast to the popular “sea of qubits” model which allows compu-

tation at every qubit. Our results show up to a 13X increase in density, particularly important in addressing our primary goal, and a speedup of about 8. The large area improvement brings the engineering of a quantum architecture closer to the capabilities of current implementation technologies.

The choice of quantum error correction codes (ECC) influences our results and the architecture. In our specialized architecture analysis, we use the previously considered Steane  $[[7, 1, 3]]$  code [3] and utilize a newly optimized Bacon-Shor  $[[9, 1, 3]]$  code [4, 5]. The  $[[9, 1, 3]]$  code, though larger than the  $[[7, 1, 3]]$  code since it uses more physical qubits to encode a single logical qubit, requires far fewer resources for error-correction [6], thus reducing the overall area and increasing the speed.

Furthermore, we find that communication is generally dominated by computation for error correction. This computation allows us to absorb the cost of moving data between different regions of the architecture. Error correction is so substantial, in fact, that quantum computers do not suffer from the *memory wall* faced by conventional computers. Thus our dense structure with a communication infrastructure based on our prior work [1] can accommodate applications with highly-demanding communication patterns.

In summary, the **contributions** of this work are: 1) Our specialized architecture, the CQLA, successfully tackles the issue of size, which has been the biggest drawback facing large-scale realizable quantum computers. 2) We show that current parallelism in quantum algorithms is inherently limited and consideration of physical resources and data movement restrict it even further. 3) We present and analyze the abstractions of memory, cache and computation units for a quantum computer; based on the insight that we can reduce reliability for the compute units and cache without sacrificing overall computation fidelity. This approach helps us significantly increase the performance of the system.

The paper is organized as follows. Section 2 provides a background of the homogeneous QLA architecture and the low-level microarchitecture assumptions of our system. Section 3 motivates the specialized CQLA architecture and introduces the architectural abstractions. Thereafter we discuss how the Steane and Bacon-Shor error correction codes affect the design of the CQLA. Results and analysis of our abstractions are the focus of section 5 following which we provide details of computation versus communication requirements of the most widely accepted quantum applications. We end with future directions in Section 7 and our conclusions in Section 8.

## 2 Background

Our architectural model is built upon our previous work on the Quantum Logic Array (QLA) architecture [1]. The

QLA architecture is a hierarchical array-based design that overcomes the primary challenges of scalability for large-scale quantum architectures. It is a homogeneous, tiled architecture with three main components: logical qubits implemented as self-contained computational tiles structured for quantum error error correction; trapped atomic ions as the underlying technology; finally, teleportation-based communication channels utilizing the concept of quantum repeaters to overcome the long-distance communication constraints.

### 2.1 The Logical Qubit

The basic structure of the QLA, our prior work, implements a fault-tolerant quantum bit, or a *logical qubit* as a self-contained tile whose underlying construction is intended for quantum error correction, by far the most dominant and basic operation in a quantum machine [7]. Quantum error correction is expensive because arbitrary reliability is achieved by recursively encoding physical qubits at cost of exponential overhead. Recursive error correction works by encoding  $N$  physical ion-qubits into a known highly-correlated state that can be used to represent a single logical data qubit. This data qubit is now at level 1 recursion and may have the property of being in a superposition of “0” and “1” much like a single physical qubit. Encoding once more we can create a logical qubit at level 2 recursion with  $N^2$  physical ion-qubits. With each level,  $L$ , of encoding the probability of failure of the system scales as  $p_0^{2^L}$ , where  $p_0$  is the failure rate of the individual physical components given a fault-tolerant arrangement and sequence of operations for the lower level components. The ability to apply logical operations on a logical qubit without the need to decode and subsequently re-encode the data is key to the existence of fault-tolerant quantum microarchitecture design, where arbitrary reliability can be efficiently reached through recursive encoding.

The logical qubits in the QLA are arranged in a regular array fashion, connected with a tightly integrated repeater-based [8] interconnect. This makes the high-level design of the QLA very similar to classical tile based architectures. The key difference is that the communication paths must account for data errors in addition to latency. Integrated repeaters known as *teleportation islands* redirect qubit traffic in the 4 cardinal directions by teleporting data from one island to the next. This interconnect design is one of the key innovative features of QLA architecture, as it allows us to completely overlap communication and computation, thus eliminating communication latency at the application level of the program.

Anticipating technology improvements in the near future we found that for performing large, relevant instances of Shor’s factoring algorithm, sufficient reliability is achieved

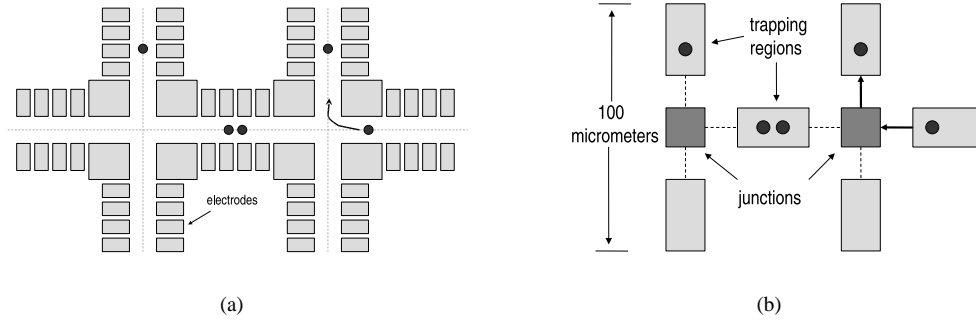


**Figure 1.** (a) A simple schematic of the basic elements of a planar ion-trap for quantum computing. Ions are trapped in any of the trapping regions shown and ballistically shuttled from one trapping region to another. When two ions are together a two-qubit gate can be performed. (b) Our abstraction of the ion-trap layout. Each trapping region can hold up to two ions for two-qubit gates. The trapping regions are interconnected with the crossing junctions which are treated as a shared resource.

at level 2 encoding per logical qubit using the Steane  $[[7, 1, 3]]$  error correction code [9]. In the QLA, computation could occur at any logical qubit and each logical gate is followed by an error correction procedure. To preserve homogeneity and maximum flexibility for large-scale applications each logical qubit was accompanied by all necessary error correction auxiliary qubit resources such that computational speed was maximized. This amounted to a (1 : 2) ratio between logical data qubits and ancillary qubits.

## 2.2 Low-Level Physical Architecture Model

At the lowest level our architecture design is based on the ion-trap technology for quantum computation. Initially proposed by Cirac and Zoller in 1995 [10], the technology uses a number of atomic ions that interact with lasers to quantum compute. Quantum data is stored in the internal electronic and nuclear states of the ions, while the traps themselves are segmented metal traps (or electrodes) that allow individual ion addressing. Two ions in neighboring traps can couple to each other forming a linear chain of ions whose vibrational modes provide qubit-qubit interaction used for multi-qubit quantum gates [11, 12]. Together with single bit rotations this yields a universal set of quantum logic gates. All quantum logic is implemented by applying lasers on the target ions, including measurement of the quantum state [13, 14, 15, 16]. Sympathetic cooling ions absorb vibrations from data ions, which are then dampened through laser manipulation [17, 18]. Recent experiments [19, 20, 21] have demonstrated all the necessary components needed to build a large-scale ion-trap quantum information processor. Finally, multiple ions in different traps can be controlled by focusing lasers through MEMS mirror arrays [22].

Operation	Time $\mu$ s now(future)	Failure Rate now(future)
Single Gate	1 (1)	$10^{-4}$ ( $10^{-8}$ )
Double Gate	10 (10)	0.03 ( $10^{-7}$ )
Measure	200 (10)	0.01 ( $10^{-8}$ )
Movement	20 (10)	$0.005 (5 \times 10^{-8})/\mu$ m
Split	200 (0.1)	
Cooling	200 (0.1)	
Memory time	10 to 100 sec	
Trap Size	$\sim 200 (1-5) \mu$ m	

**Table 1.** Column 1 gives estimates for execution times for basic physical operations used in the QLA model. Currently achieved component failure rates are based on experimental measurements at NIST with  ${}^9\text{Be}^+$  ions, and using  ${}^{24}\text{Mg}^+$  ions for sympathetic cooling [14, 12]. All parameters are followed by their projected parameters in parenthesis, extrapolated following recent literature [23, 24, 25], and discussions with the NIST researchers; these estimates are used in modeling the performance of our architecture.

Figure 1 shows a schematic of the physical structure of an ion trap computer element. In Figure 1(a) we see a single ion trapped in the middle trapping region. Trapping regions are the locations where ions can be prepared for the execution of a logical gate, which is implemented by an external laser source pulsed on the ions in the trap. In the figure we see an ion moving from the far right trapping region to the top-right for the execution of a two-bit logical operation.

Figure 1(b) demonstrates our abstraction of the physical ion-trap layout. The layout can be represented as a collection of trapping regions connected together through shared junctions. A fundamental time-step, or a clock cycle, in an ion-trap computer will be defined as any physical, un-

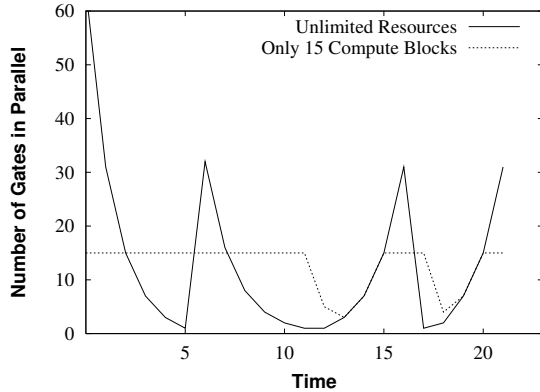


**Figure 2.** For a 64-qubit adder, the amount of parallelism that can be extracted when resources are unlimited, and when the number of gates per cycle are limited. This figure shows that if 15 gates, or an unlimited number of gates could be performed in each cycle, the total runtime would remain the same. compute blocks increases.

encoded logic operation (one-bit or two-bit), a basic move operation from one trapping region to another, and measurement. Table 1 summarizes current experimental parameters and corresponding optimistic parameters for ion-traps. In our subsequent analysis we will assume that each *clock cycle* for a fundamental time-step has a duration of  $10 \mu\text{s}$ , failure rates are  $10^{-8}$  for single-qubit operations and measurement,  $10^{-7}$  for CNOT gates [25], and order of  $10^{-6}$  per fundamental move operation. The movement failure rate is expected to improve from what it is now as trap sizes shrink and electrode surface integrity continues to improve. We will assume trap sizes of  $5 \mu\text{m}$  each [26], and on the order of 10 electrodes per trapping region [27], which gives us a trapping region dimension (including the junction) of  $50 \mu\text{m}$ . The parameters chosen for our study are optimistic compared to [28] and [29]. Both of those papers, assume more pessimistic near term parameters which are useful for building a 100 bit prototype, but probably not a scalable quantum computer that can factor 1024-bit numbers using Shor’s algorithm. Based on the quantum computing ARDA roadmap [23], we feel justified in using aggressive parameters when looking 10-15 years into the future.

### 3 Architectural Abstractions

This section motivates the need for a compact architecture for quantum processors and describes our design the CQLA (Compressed Quantum Logic Array). We discuss how separation into memory and compute regions benefits the CQLA and then present our quantum memory hierarchy.

### 3.1 Motivation

Conventional quantum processor designs are based on the *sea-of-qubits* design and allow computation to take place anywhere in the processor. This design philosophy follows the idea of maximum parallelism and is employed in our previous work [1]. The area consumption of such a design however, is untenably large, about  $1 \text{ m}^2$  to factor a 1024-bit number.

When we consider the amount of available parallelism in quantum applications, we discover that much is to be gained by limiting computation to a specifically designated location. The remaining area can be optimized for storage of quantum data. A good example for the benefit of specialization in quantum applications is the Draper carry-lookahead quantum adder [30], which forms a basic component of Shor’s quantum factoring algorithm [31]. Figure 2 shows that providing unlimited computational resources for a 64-bit adder does not offer a performance benefit over limiting the computation to 15 locations. As illustrated in Section 2, the number of ancillary resources for each data location where computation is allowed is twice as large. In this example, by providing only 15 compute locations instead of 64, we can reduce the area consumed by the adder by approximately *half* and yet have no change in performance.

### 3.2 Specialized Components

The facts that qubits in an ion-trap quantum processor have *large lifetimes* when idle, allows us to improve logical qubit density in the memory. Qubits in memory can wait for a longer time period between two consecutive error corrections. We use this to significantly reduce the error correction ancillary resources in memory, thereby reducing its density. The majority of computation, on the other hand, is an interaction between two distinct logical qubits. To maintain adequate system fidelity, every gate must be followed by an error correction procedure. Consequently, a quantum processor spends most of its time performing error correction and the compute regions are designed to allow fast error correction by providing a greater number of ancilla in the logical qubits. Figure 3(a) shows a specialization into compute and memory regions. The ratio of (data:ancilla) can be seen to be (8 : 1) for memory and (1 : 2) for the compute region.

While specialization helps address our primary goal of reducing size, it can possibly also reduce performance. In Section 5 we show how judiciously choosing the size of the compute region helps maintain adequate performance while simultaneously reducing size .

### 3.3 Quantum Memory Hierarchy

Another important architectural design choice is the effect of the error correction code chosen in both the mem-

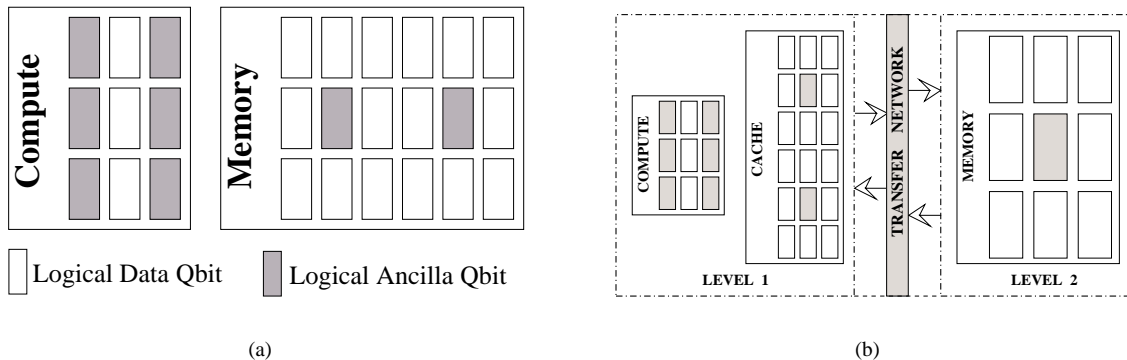


**Figure 3.** (a) Memory is denser since it has fewer ancilla qubits. The figure shows 3 data qubits in the compute block which take the same area as 8 data qubits in memory. In the CQLA each compute block holds nine 9 data qubits and 18 ancilla. Both compute and memory are at level 2 encoding. (b) Memory is at level 2 encoding, while the compute and cache are at level 1 encoding. The complete CQLA consists of memory at level 2, compute regions at level 2, and also a cache and compute region at level 1.

ory and the compute regions. Error correction is the most dominant procedure and the resources used increase exponentially with each level of concatenation. In addition to resources, the time to error correct increases exponentially with each level of concatenation. The benefits of concatenated error correction are that the reliability of each operation increases double exponentially, thus allowing for a greater number of total operations to be performed. For any application, all logical qubits are not being acted upon by gates for the entire duration of the algorithm. In fact, just like classical computers, data locality is a common phenomenon. This implies that a logical qubit could start at level 2 encoding, be encoded at level 1 during the peak in its activity and return to level 2 when idle.

We now introduce a quantum memory hierarchy, in addition to the specialized design. Memory at level 2, which is optimized for area and reliability will be inherently slower than a computational structure, at level 1, optimized for gate execution. This necessitates the need for a cache that can alleviate the need for constant communication.

Figure 3(b) outlines this approach. The separation between memory and compute regions. The cache and the compute regions here are similar to Figure 3(a) in every way save that they are at a lower level of encoding. In the memory hierarchy, memory and cache have a similar design, only memory is at a higher level of encoding, and hence is slower and much more reliable. The critical feature here is the **transfer network** which is more complicated and hence slower than the teleportation channels described above. The transfer network comes into play only when we change the encoding of a logical qubit. For all other communication

(within compute blocks, between cache and compute blocks and within memory) teleportation is still the chosen mechanism. Section 4 describes how the transfer process is performed in a fault-tolerant manner.

## 4 Error Correction and Code Transfer

In this section we describe the cost of the error correction circuits and code-transfer networks we use when a specific physical layout is considered. Section 2.2 describes in detail our technology parameters, which we find to be necessary for such a large-scale architecture. These parameters allow the large scalability to be achieved because the physical component failure rates are below the threshold value needed for efficient error correction [32].

### 4.1 Error Correction Codes

Some of the best error correction codes (ECC) are ones that use very few physical qubits, and allow “easy” fault-tolerant gate implementations. A requirement of a fault-tolerant system is that computation proceeds without decoding the encoded data. Thus logical gates are implemented directly on encoded qubits, ensuring that errors introduced during the gate can be corrected. Many code choices for EC allow *transversal* logical gate implementation, which means that the same physical gate acts on each lower-level qubit.

Each logical quantum gate is preceded and followed by an error correction procedure. The EC procedure works by encoding ancillary qubits in the logical “0” state of the data and interacting the data and the ancilla. The interaction causes errors in the data to propagate to the ancilla and to

be detected when the ancilla is measured. There are several very important logical gates that we must consider during error correction. The bit-flip gate,  $X$  flips the value of the qubit by reversing the probabilities between its “0” component and its “1” component. The phase-flip gate,  $Z$ , acts only on the qubit’s “1” component by changing its sign. The most important gate is the controlled- $X$  gate (denoted as the CNOT gate) which flips the state of the target qubit whenever the state of the control qubit is set. Errors on the data can be understood as the product of phase-flips and a bit-flips. A syndrome is extracted for each types of error. We only present the cost of error correction networks and details relevant to building a large-scale architecture. The interested reader can refer to the literature for additional theoretical information [33].

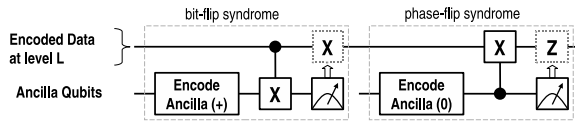


**Figure 4.** A high-level view of an error correction sequence. Two syndromes for bit-flip and phase-flip errors are extracted.

Figure 4 is a simple schematic of the general error correction procedure, where time flows from left to right and each line represents the evolution of an encoded logical qubit. An error correction code is labeled by  $[[n, k, d]]$ , encoding  $k$  logical qubits into  $n$  qubits and correcting  $(d - 1)/2$  errors. If our target reliability is such that we require  $L$  levels of recursion, each line in Figure 4 represents  $n^L$  level zero qubits. For the bit-flip error syndrome the ancilla are encoded into the logical  $(0 + 1)$ , and the transversal CNOT gate, which is essentially  $n$  level  $(L - 1)$  transversal CNOT gates of which the ancillary qubits are targets. Each of the lower level CNOT gates is followed by a lower level error correction unless the lower level is zero. In our architecture analysis we provide information about two error correcting codes: the Steane  $[[7, 1, 3]]$  code [9], and an improved version of the Shor  $[[9, 1, 3]]$  code [34] denoted as the Bacon-Shor code [4, 5, 6].

**The Steane  $[[7, 1, 3]]$  Code** encodes 1 qubit into 7 qubits, and is the smallest error correction code allowing transversal gate implementation for all gates involved in concatenated error correction algorithms. The addition of the  $T$  phase gate, which is harder to implement, provides universal quantum logic using the  $[[7, 1, 3]]$  error correcting code. For this reason it was used as the underlying error correcting code in the analysis of the QLA architecture [1]. It consists of 7 data ions which encode our logical level 1 qubit with 14 ancillary ions used for error correction, seven of which are used in the error correction and the other verify the ancilla.

Error Correction Metric Summary		
Architecture Metric	Error Code - Level	Value
EC Time (seconds)	$[[7, 1, 3]]$ - L1	$3.1 \times 10^{-3}$
	$[[7, 1, 3]]$ - L2	0.3
	$[[9, 1, 3]]$ - L1	$1.2 \times 10^{-3}$
	$[[9, 1, 3]]$ - L2	0.1
Qubit Size ( $mm^2$ )	$[[7, 1, 3]]$ - L1	0.2
	$[[7, 1, 3]]$ - L2	3.4
	$[[9, 1, 3]]$ - L1	0.1
	$[[9, 1, 3]]$ - L2	2.4
Transversal Gate Time (seconds)	$[[7, 1, 3]]$ - L1	$6.2 \times 10^{-3}$
	$[[7, 1, 3]]$ - L2	0.5
	$[[9, 1, 3]]$ - L1	$2.4 \times 10^{-3}$
	$[[9, 1, 3]]$ - L2	0.2
Size, number of logical qubits	$[[7, 1, 3]]$ - L1	7
	$[[7, 1, 3]]$ - L1(ancilla)	21
	$[[7, 1, 3]]$ - L2	49
	$[[7, 1, 3]]$ - L2(ancilla)	441
	$[[9, 1, 3]]$ - L1	9
	$[[9, 1, 3]]$ - L1(ancilla)	12
	$[[9, 1, 3]]$ - L2	81
	$[[9, 1, 3]]$ - L2(ancilla)	298

**Table 2.** Error Correction Metric Summary. Given the fact that we use optimistic ion-trap parameters all numbers are estimates and are thus rounded to only one significant digit.

Considering communication, the level 1 error correction circuit in will take 154 cycles, where each cycle is in the order of 10 microseconds, and can be as large as 0.003 per error correction procedure at level 1. A level 2  $[[7, 1, 3]]$  qubit will be composed of 7 level 1 data qubits and 7 level 1 ancilla qubits - there is no need for verification ancilla at  $L = 2$ . The size of a level 2 qubit will be  $3.4 mm^2$ , and a fully serialized error correction will last approximately 0.3 seconds (this is two orders of magnitude more than the time to error correct at level 1).

**Bacon-Shor  $[[9, 1, 3]]$  Code:** The  $[[9, 1, 3]]$  code was the first error correcting code to be discovered for arbitrary errors [34]. Recent observations make this code faster and spatially smaller than the  $[[7, 1, 3]]$  code [4, 5, 6]. The compact structure of the physical layout for the  $[[9, 1, 3]]$  code significantly improves communication requirements. At level 1 the error correction time is only 0.001 seconds and 0.1 seconds at level 2. The level 2 qubit size is approximately  $2.4 mm^2$ . Table 2 summarizes the error correction we have used and their parameters for some useful architecture metrics.

## 4.2 Code Transfer Networks: Overview

One of the most interesting components of the memory hierarchy are the code transfer regions. This region transfers data encoded in code C1 to a second code C2 with-

(seconds)	7-L1	7-L2	9-L1	9-L2
7-L1	0	0.6	0.02	0.2
7-L2	1.3	0	1.3	1.5
9-L1	0.01	0.5	0	0.1
9-L2	0.4	0.9	0.4	0

**Table 3.** Transfer network latency for a combination of the  $[[7, 1, 3]]$  and  $[[9, 1, 3]]$  codes.

out the need to decode. Figure 4.2 illustrates this concept. The transfer network *teleports* the data in C1 to C2, where C1 and C2 may be any two error correcting codes. The code teleportation procedure works much the same way as standard data teleportation that is used for communication. A correlated ancillary pair is prepared first between C1 and C2 through the use of a multi-qubit cat-state (i.e. “(00...0 + 11...1)”). The data qubit interacts with the equivalently encoded ancillary qubit through a CNOT gate, and the two are measured. Following the measurement the state of the data is recreated at the C2 encoded ancillary qubit. This process is required every time we transfer a qubit from memory to the cache or vice-versa. Table 3 summarizes the times for different code transfer combinations between levels 1 and 2 for the  $[[7, 1, 3]]$  and the  $[[9, 1, 3]]$  codes.

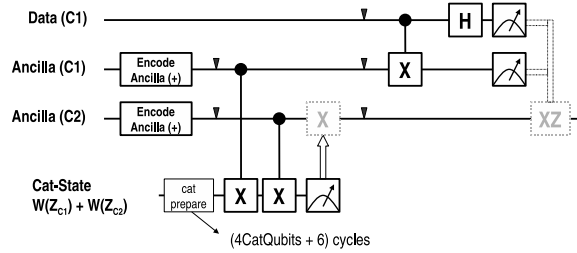


**Figure 5.** Code Teleportation Network from Code 1 (C1) to Code 2 (C2) C1 and C2 can even be the same error correcting code, but different levels of encoding. The solid triangles denote an error correction step.

## 5 CQLA Analysis and Results

This section provides analysis of the abstractions presented in

to perform quantum modular exponentiation.

### 5.1 Specialization into Memory

We now analyze our design, the CQLA, when it separates the quantum processor into memory and compute regions. High density in memory is achieved by greatly reducing the ratio of logical data qubits to logical ancilla

qubits, which is (8 : 1) in memory and is (1 : 2) in the compute regions. This greatly reduces overall area since prior work had a ratio of (1 : 2) throughout the architecture. Thus the memory is denser, but slower, which is permissible due to the large memory wait times 1.

Quantum modular exponentiation is the most time consuming part of Shor’s algorithm, and the Draper carry-lookahead adder is its most efficient implementation. This adder comprises single qubit gates, two qubit cnot gates and three qubit toffoli gates and is dominated by toffoli gates. The time to perform a single fault-tolerant toffoli is equal to the time for fifteen two qubit gates, each of which is followed by an error-correction step. Table 5.1 shows the savings that can be achieved when using denser memory. Note that performance is minimally impacted for the Steane Code as we exploit the limited parallelism in the adder. We address the parallelism available within the application itself and determine the number of compute blocks to maximally exploit this parallelism with change with problem size. Figure 6(a) shows how for a fixed problem size, utilization of each compute block decreases with an increase the number of compute blocks. Clearly, the decrease in utilization is offset by the increase in overall performance. Thus the challenge here is to find the *balance* between utilization and performance.

We compare all our results to [1], which used only the Steane ECC. Since the Bacon-Shor ECC uses fewer overall resources 2 and allows faster error-correction, a design based on these codes not only is much smaller, but is also faster. The CQLA, thus reduces area required by a **factor of 9** with minimal performance reduction for the Steane ECC and by a **factor of 13** with a **speedup of 2** when using the Bacon-Shor ECC. To compare the relative merit our design choices, we use the *gain product* which can be defined by  $GP = (Area_{old} * AdderTime_{old}) / (Area_{CQLA} * AdderTime_{CQLA})$  where *AdderTime* is the average time per adder for modular exponentiation. The gain product indicates the improvement in system parameters relative to our prior work, the QLA. The higher the gain product, the better the collective improvement in area and time of our system.

**Communication Issues:** Toffoli gates cannot be directly implemented on encoded data and have to be broken down into multiple two qubit gates. Performing a fault-tolerant Toffoli between three logical qubits requires extra logical ancilla and logical cat-state qubits. The flow of data between these nine qubits to complete a single toffoli forms the most intense communication pattern during the entire addition operation. To study the bandwidth requirements during the toffoli gates, we developed a scheduler that would try to have all the requirements for communication (creating EPR pairs, transporting and purifying them)

Input Size	Compute Blocks	Area Reduced (Factor of)		SpeedUp		Gain Product	
		St-Code	BSr-Code	St-Code	BSr-Code	St-Code	BSr-Code
32-bit	4	6.69	9.80	0.54	1.47	3.61	14.41
	9	3.22	4.74	0.97	2.9	3.14	13.74
64-bit	9	6.36	9.32	0.70	1.92	4.45	17.70
	16	3.79	5.56	0.98	3.0	3.71	16.68
128-bit	16	7.24	10.6	0.72	1.97	5.24	20.88
	25	4.90	7.17	0.96	2.84	4.70	20.36
256-bit	36	6.65	9.47	0.92	2.51	6.12	23.68
	49	5.07	7.43	0.98	2.98	4.96	22.14
512-bit	64	7.42	10.87	0.92	2.50	6.80	27.18
	81	6.06	8.87	0.98	2.91	5.94	25.81
1024-bit	<b>100</b>	<b>9.14</b>	<b>13.4</b>	<b>0.80</b>	<b>2.19</b>	<b>7.35</b>	<b>29.35</b>
	121	7.81	11.45	0.97	2.65	7.60	30.34

**Table 4.** For various size inputs, this table shows how the CQLA performs for Modular Exponentiation. The space saved due to compressing the memory blocks and separating memory and compute regions is shown as compared to prior work [1]. St-Code is the Steane ECC and BSr-Code is the Bacon-Shor code. The Gain Product is compared with our prior work, the QLA, which has a Gain Product of 1.0.

in place while the logical qubit to be transported was undergoing error-correction after completion of the previous gate. With bandwidth of one channel, it was possible to overlap communication with computation for the Steane  $[[7, 1, 3]]$  code. To enable this overlap when using the Bacon-Shor code, the required bandwidth was three channels. Table 2 shows that while a logical qubit encoded in the Bacon-Shor code is smaller when ancilla are considered; it has more data qubits than the Steane code. Since only data qubits are involved during teleportation, the time for teleporting a logical qubit in the Bacon-Shor code is greater. In addition, the Bacon-Shor codes take far fewer error-correction cycles. These two factors push its bandwidth requirement higher. Note that the higher bandwidth is accounted for in results of Table 5.1.

**Superblocks:** In the CQLA, several compute blocks together form compute superblocks. This is done to exploit the locality inherent to an application. Having larger superblocks also increases the perimeter bandwidth between the compute and memory regions of the CQLA. This increase in bandwidth of a larger superblock is offset by the much greater increase in communication required. Our intuition tells us that at a certain point, it may be more efficient to have multiple small superblocks instead of one large superblock. To determine this number concretely, we plot the change in bandwidth required against change in bandwidth available. Figure 6(b) shows the cross-over point is 36 compute blocks per superblock, immaterial of what error correction code is used. Thereafter it is no longer beneficial to increase the size of an individual compute superblock.

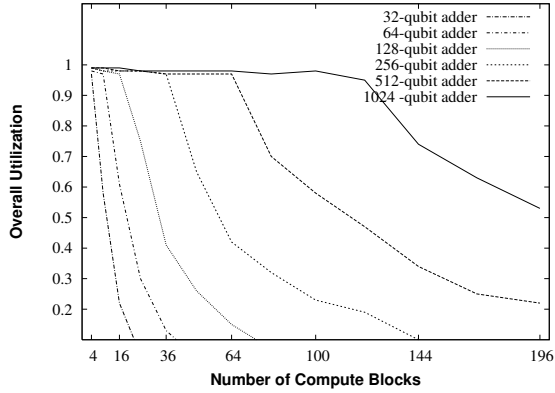
## 5.2 Memory Hierarchy

Reducing the encoding level of the compute region will dramatically increase its speed. Recall that resources, time and reliability all increase exponentially as we increase the level of encoding. With the compute region at level 1 and memory at level 2, the challenge is the very familiar one of the CPU being an order of magnitude faster than the memory. To maximize the benefit of a much faster compute region, we introduce the quantum memory hierarchy. In our hierarchy, the memory is at level 2 encoding (slow and reliable), cache is at level 1 (faster, less reliable) and the compute region is also at level 1 (fastest and same reliability as cache). The difference in speed between the compute region and the cache is due to a greater number of ancilla in the compute region.

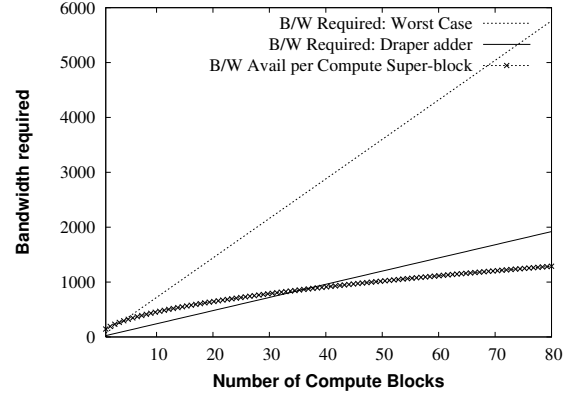
To study the behavior of the CQLA with a cache and multiple encoding levels, we developed a simulator that models a cache. The simulator takes into account the computation cost in both encoding levels and also the cost of transferring logical qubits between encoding levels. The application under consideration is still the Draper carry-lookahead adder. Input to the simulator is a sequence of instructions; each instruction is similar to assembly language and describes a logical gate between qubits. We have written generators that output this code in a form that can take advantage of an architecture with maximal parallelism.

When the simulator runs this code in the sequence intended by the Draper carry-lookahead adder, the cache hit-rate is limited to 20%. To improve the hit-rate, we utilize the following optimized approach. Since we are scheduling statically, the instruction fetch window for the simulator





(a)



(b)

**Figure 6.** (a) Change in utilization as the number of compute blocks increases. (b) The point of intersection of the two bottom curves is the optimal size of a compute superblock. These two curves are bandwidth required (at the perimeter of the compute superblock) in modular exponentiation and bandwidth available. The third steep curve, is the worst case bandwidth required.

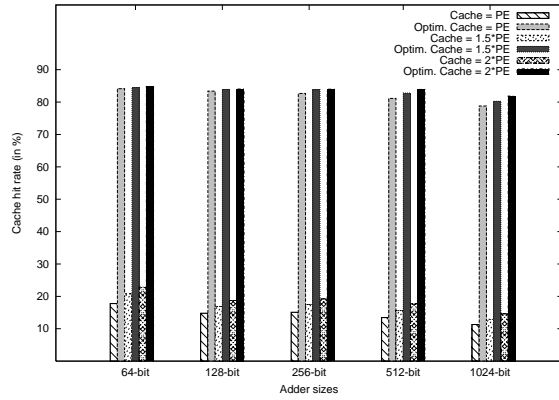


**Figure 7.** Shows the cache hitrate for different adders when both cache and compute region are at Level 1 recursion. Largest cache considered holds twice the number of logical qubits as the compute block. Results for both the non-optimized version and the optimized version are shown.

can be the whole program. The simulator takes advantage of this by first creating a dependency list of all input instructions. Then it carefully selects the next instruction such that probability of finding all required operands in the cache is maximized. This optimized fetch yields a cache hit-rate of almost 85% immaterial of adder size and cache size. The replacement policy in the cache is least recently used. Figure 7 shows the cache hit-rates for different sized adders for the non-optimized and optimized instruction fetch approaches. If  $n$  is the number of logical qubits in the compute region, the cache sizes we studied were  $n$ ,  $1.5n$  and  $2n$ . As the graph shows, the increase in hit-rate is more pronounced due to the optimized fetch than increasing cache size. For the CQLA, we thus employ a cache size of twice the number of qubits in the compute region. The high hit-rate means the transfer networks will not be overwhelmed.

**Fault-tolerance with multiple encoding levels:** A quantum computer running an application of size  $S = KQ$ , where  $K$  is the number of time-steps and  $Q$  is the number of logical qubits, will need to have a component failure rate of at most  $P_f = 1/KQ$ . To evaluate the expected component failure rate at some level or recursion we use Gottesman's estimate for local architectures [35] shown in Equation 1 below.

$$P_f = \frac{1}{cr^2 r^L} (cr^2 p_0)^{2L} = \frac{p_{th}}{r^L} (p_{th}^{-1} p_0)^{2L} \quad (1)$$

The value for  $r$  is the communication distance between level 1 blocks which are aligned in QLA to allow  $r = 12$  cells on average and  $L$  denotes the level of recursion. The

Par Xfer	Adder Size	L1 SpeedUp	L2 SpeedUp	Adder SpeedUp	Area Reduced	Gain Product
Steane $[[7, 1, 3]]$ Code						
10	256	17.417	0.98	6.25	5.07	31.68
	512	17.41	0.97	6.33	6.06	38.38
	1024	18.18	0.88	<b>4.93</b>	<b>9.14</b>	<b>45.06</b>
5	256	10.409	0.98	4.05	5.07	24.99
	512	10.408	0.97	4.04	6.06	24.48
	1024	10.96	0.88	<b>2.94</b>	<b>9.14</b>	<b>26.87</b>
Bacon-Shor $[[9, 1, 3]]$ Code						
10	256	9.61	1.53	5.92	7.43	43.99
	512	9.61	2.28	8.82	8.87	78.23
	1024	10.15	2.00	<b>8.10</b>	<b>13.4</b>	<b>108.53</b>
5	256	5.17	1.53	3.66	7.43	27.19
	512	5.17	2.28	5.45	8.87	48.37
	1024	5.49	2.00	<b>4.99</b>	<b>13.40</b>	<b>66.90</b>

**Table 5.** This table shows the results of incorporating a memory hierarchy and two separate encoding levels. Depending on the number of parallel transfers possible between memory and cache, we can expect different speedup values for the adder at level 1. This combined with results from Table 5.1 give us the final Gain Product. Comparatively, prior work has an Gain Product number of 1.0.

threshold failure rate,  $p_{th}$ , for the Steane  $[[7, 1, 3]]$  circuit accounting for movement and gates was computed in [36] to be approximately  $7.5 \times 10^{-5}$ . Taking as  $p_0$  the average of the expected failure probabilities given in Table 1, and using Equation 1, we find that for our system to be reliable it can spend **only 2%** of the total execution time in level 1. Recall that error-correction is the most frequently performed operation in the CQLA. For the Steane code, level 2 error correction takes 0.3 sec and level 1 takes  $3.1 \times 10^{-3}$  sec, which is approximately 1% of the level 2 time. Thus if all operations performed by the CQLA were equally divided between level 1 and level 2 operations, the system will maintain its fidelity. The Bacon-Shor ECC can be analyzed in a similar manner and their results are more favourable due to a higher threshold.

The CQLA architecture now consists of a memory at level 2, a compute region also at level 2, a cache and a compute region at level 1 and transfer networks for changing the qubit encoding levels. Since quantum modular exponentiation is performed by repeated quantum additions, we could perform half of these additions completely in level 2 and the other half in level 1. To comfortably maintain the fidelity of the system, we perform one level 1 addition for every two level 2 additions. The resulting increase in performance is shown in Table 5.

## 6 Application Behavior

In this section compute and memory are at level 2 encoding. Contrary to traditional silicon based processors, in the

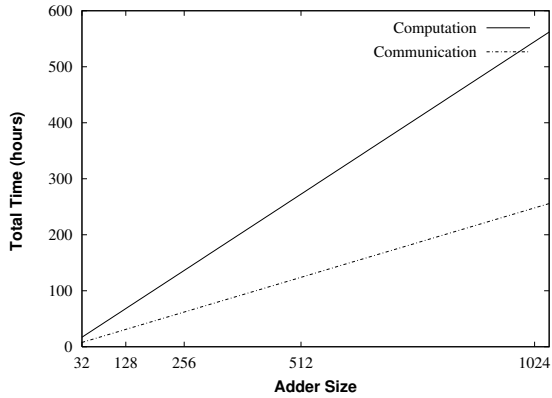
CQLA a single communication step does not take longer than the computation of a single gate. The reason behind this phenomenon is the lack of reliability of quantum data, which forces us to perform an error-correction procedure after each gate. The time to complete a fault-tolerant Toffoli is about 20 times greater than a two-qubit CNOT gate. The applications we study are modular exponentiation and the quantum fourier transform.

### 6.1 Shor’s Algorithm

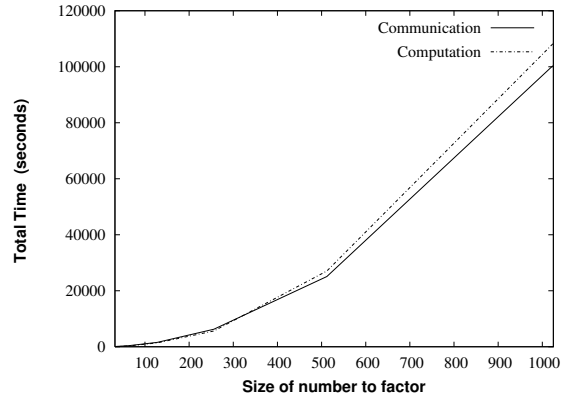
Shor’s algorithm is the most celebrated of quantum algorithms due to its potential exponential advantage over conventional algorithms and its application to breaking public-key cryptography [31]. Shor’s algorithm is primarily composed of two parts, the modular exponentiation and the quantum fourier transform.

**Modular Exponentiation:** The execution of modular exponentiation is dominated by Toffoli gates. To keep the compute block from having to wait for qubits, and hence stalling, the bandwidth around the perimeter of the compute block has to accommodate the transfer of three qubits to and from memory. Intuitively, since the CQLA is a mesh, and the bottleneck in bandwidth will be at the edge of the compute blocks, having adequate bandwidth at this edge is sufficient for the rest of the mesh.

Based on the communication results from [1], we calculate that a 2 channels on the perimeter of the compute block would provide adequate bandwidth for all required communication. We compute the time required for all communica-



(a)



(b)

**Figure 8.** Total communication and computation times for the two components of Shor’s algorithm, (a) Modular Exponentiation (b) Quantum Fourier Transform (QFT). Although communication is significant in the QFT, Modular exponentiation dominates Shor’s algorithm. Both these results are for the Bacon-Shor code

tion steps and compare it against the total computation time for differently sized adders. The result is shown in 8(a) and demonstrates that communication requirements do not adversely impact the design.

**Quantum Fourier Transform:** While the Quantum Fourier Transform (QFT) comprises a small fraction of the overall Shor’s algorithm, it requires all-to-all personalized communication between data qubits. In addition, it uses only one-qubit and two-qubit gates which consume much less time. As a result, studying the performance of the QFT gives us an insight into how the CQLA will behave when faced with an communication heavy and a computation light application.

In the worst case, all nine data qubits (maximum capacity of the compute block) would have to be transferred to or from memory simultaneously.

Between compute blocks, the QFT’s all-to-all personalized communication must be supported on the CQLA mesh network. We leverage the vast amount of prior work done in studying mesh networks, and employ a near-optimal algorithm proposed in [37]. The total time for communication for varying problem sizes is shown in figure 8(b). Note that while communication time is a little less, it closely tracks the computation time for all problem sizes. This is due to the difference in time to error correct a single logical qubit and the time to transport a single qubit; which stays constant immaterial of the problem size.

## 7 Future Work

A high-level goal of this work is to build abstractions from which architects and systems designers can examine open issues and help guide the substantial basic science and engineering under investment towards building a scalable quantum computer. The primary focus of our work has been system balance. The driving force in this balance has been application parallelism. A key open issue is the restructuring of quantum algorithms to manage this parallelism in the context of system balance. From an architectural point of view, the most relevant abstract properties are density of functional components, the memory hierarchy and communication bandwidth.

While our work has focused on trapped ions, most scalable technologies will have a similar two-dimensional layout where our techniques can be easily applied. This is because the density is determined by the ratio of data to ancilla rather than physical details of the underlying technology.

For ion-traps, lasers can also be a control issue. We plan to study how our architecture can minimize the number of lasers and minimize the power consumed by each laser, since power is proportional to fanout. Efficiently routing control signals to all electrodes in an ion-trap is a challenging proposition, one that has not yet been considered for large systems. Currently, we perform the whole adder at the fast level 1 encoding or at the level 2 encoding; clever instruction scheduling techniques can allow us to improve performance by reducing granularity.

## 8 Conclusion

The technologies and abstractions for quantum computing have evolved to an exciting stage, where architects and system designers can attack open problems without intimate knowledge of the physics of quantum devices. We explore the amount of parallelism available in quantum algorithms and find that a specialized architecture can serve our needs very well. The CQLA design is an example where architectural techniques of specialization and balanced system design have led to up to a **13X** improvement in density and a **8X** increase in performance, while preserving fault tolerance. We hope that further application of compiler and system optimizations will lead to even more dramatic gains towards a scalable, buildable quantum computer.

## References

- [1] T. S. Metodi, D. D. Thaker, A. W. Cross, F. T. Chong, and I. L. Chuang, "A quantum logic array microarchitecture: Scalable quantum data movement and computation," *Proceedings of the 38th International Symposium on Microarchitecture MICRO-38*, 2005.
- [2] W. Wootters and W. Zurek, "A single quantum cannot be cloned," *Nature* **299**, pp. 802–803, 1982.
- [3] A. M. Steane, "Space, time, parallelism and noise requirements for reliable quantum computing," *Fortsch. Phys.* **46**, pp. 443–458, 1998.
- [4] D. Bacon, "Operator quantum error correcting subsystems for self-correcting quantum memories," *quant-ph/0506023*, 2005.
- [5] D. Poulin, "Stabilizer formalism for operator quantum error correction," *quant-ph/0508131*, 2005.
- [6] P. Aliferis *Unpublished work based on private conversations with Andrew Cross.*, 2006.
- [7] M. Oskin, F. Chong, and I. Chuang, "A practical architecture for reliable quantum computers," *IEEE Computer*, January 2002.
- [8] W. Dur, H. J. Briegel, J. I. Cirac, and P. Zoller, "Quantum repeaters based on entanglement purification," *Phys. Rev.* **A59**, p. 169, 1999.
- [9] A. Steane, "Error correcting codes in quantum theory," *Phys. Rev. Lett* **77**, pp. 793–797, 1996.
- [10] J. I. Cirac and P. Zoller, "Quantum computations with cold trapped ions," *Phys. Rev. Lett* **74**, pp. 4091–4094, 1995.
- [11] A. Sorensen and K. Molmer, "Entanglement and quantum computation with ions in thermal motion," *Phys. Lett. A* **62**, p. 02231, 2000.
- [12] D. Leibfried and et al., "Experimental demonstration of a robust, high-fidelity geometric two ion-qubit phase gate," *Nature* **422**, pp. 412–415, 2003.
- [13] E. Hahn, "Spin echoes," *Phys. Rev.* **80**, pp. 580–594, 1950.
- [14] D. Wineland and et al., "Experimental issues in coherent quantum-state manipulation of trapped atomic ions," *Journal of Research of NIST* **103**, pp. 259–328, 1998.
- [15] D. Kielpinski, C. Monroe, and D. Wineland, "Architecture for a large-scale ion-trap quantum computer," *Nature* **417**, pp. 709–711, 2002.
- [16] J. Porto, S. Rolston, T. Laburthe, C. Williams, and W. Phillips, "Quantum information with neutral atoms as qubits," *Phil. Trans. R. Soc. Lond.* **A361**, pp. 1417–1427, 2003.
- [17] B. Blinov, L. Deslauriers, P. Lee, M. Madsen, R. Miller, and C. Monroe, "Sympathetic cooling of trapped ions for quantum logic," *Phys. Rev. A.* **61**, p. 032310, 2000.
- [18] B. Blinov, L. Deslauriers, P. Lee, M. Madsen, R. Miller, and C. Monroe, "Sympathetic cooling of trapped cd+ isotopes," *Phys. Rev. A.* **65**, p. 040304, 2002.
- [19] M. Barrett, J. Chiaverini, T. Schaetz, J. Britton, and et. al., "Deterministic quantum teleportation of atomic qubits," *Nature* **429**, 2004.
- [20] M. Riebe, H. Haffner, C. Roos, and et. al., "Deterministic quantum teleportation with atoms," *Nature* **429**(6993), pp. 734–737, 2004.
- [21] J. Chiaverini, R. B. J. Britton, J. Jost, C. Langer, D. Leibfried, R. Ozeri, and D. Wineland, "Surface-electrode architecture for ion-trap quantum information processing," *E-Print: quant-ph/0501147*, 2004.
- [22] J. Kim, S. Pau, Z. Ma, H. McLellan, J. Gages, A. Kornblit, and R. Slusher, "System design for large-scale ion trap quantum information processor," *Quantum Information and Computation* **5**(7), 2005.
- [23] D. Wineland and T. Heinrichs, "Ion trap approaches to quantum information processing and quantum computing," *A Quantum Information Science and Technology Roadmap*, 2004. URL: <http://quist.lanl.gov>.
- [24] A. Steane, "How to build a 300 bit, 1 gop quantum computer," *arXiv:quant-ph/0412165*, 2004.
- [25] R. Ozeri and et. al., "Hyperfine coherence in the presence of spontaneous photon scattering," *arXiv:quant-ph/0502063*, 2004.
- [26] D. Wineland, D. Leibfried, M. Barrett, A. Ben-Kish, and et.al., "Quantum control, quantum information processing, and quantum-limited metrology with trapped ions," *Proceedings of the International Conference on Laser Spectroscopy (ICOLS)*, 2005.
- [27] W. K. Hensinger, S. Olmschken, D. Stick, D. Hucul, M. Yeo, M. Ac-ton, L. Deslauriers, J. Rabchuk, and C. Monroe, "T-junction ion trap array for two-dimensional ion shuttling, storage and manipulation," *E-Arxiv: quant-ph/0508097*, 2005.
- [28] S. Balensiefer, L. Kregor-Stickles, and M. Oskin, "An evaluation framework and instruction set architecture for ion-trap based quantum micro-architectures.," *ISCA-32; Madison, WI*, 2005.
- [29] R. V. Meter and M. Oskin, "Architectural implications of quantum computing technologies," *ACM Journal on Emerging Technologies in Computing Systems (JETC)* **2**(1), 2006.
- [30] T. Draper, S. Kutin, E. Rains, and K. Svore, "A logarithmic-depth quantum carry-lookahead adder," *E-Print: quant-ph/0406142*, 2004.
- [31] P. Shor, "Polynomial-time algorithms for prime factorization and discrete logarithms on a quantum computer," *35th Annual Symposium on Foundations of Computer Science*, pp. 124–134, 1994.
- [32] D. Aharonov and M. Ben-Or, "Fault tolerant computation with constant error," *Symposium on Theory of Computing (STOC 1997)*, pp. 176–188.
- [33] M. A. Nielsen and I. L. Chuang, *Quantum Computation and Quantum Information*, Cambridge University Press, Cambridge, UK, 2000.
- [34] P. W. Shor, "Scheme for reducing decoherence in quantum computer memory," *Phys. Rev. A* **54**, p. 2493, 1995.
- [35] D. Gottesman, "Fault tolerant quantum computation with local gates," *Journal of Modern Optics* **47**, pp. 333–345, 2000.
- [36] K. Svore, B. Terhal, and D. DiVincenzo, "Local fault-tolerant quantum computation," *E-Print: quant-ph/0410047*, 2004.
- [37] Y. Yang and J. Wang, "Pipelined all-to-all broadcast in all-port mesh and tori," *IEEE Transactions on Computers* **50**(10), pp. 1020–1032, 2001.